JOURNAL OF THE KOREAN ASTRONOMICAL SOCIETY
27: 81 ~ 102, 1994

THERMAL AND NON-THERMAL RADIO CONTINUUM SOURCES IN THE W51 COMPLEX

MOON, DAE-SIK AND KOO, BON-CHUL
Department of Astronomy, Seoul National University,
Seoul 151-742, Korea
(*Received Apr. 15, 1994; Accepted Apr. 22, 1994*)

ABSTRACT

We have decomposed the 11-cm radio continuum emission of the W51 complex into thermal and non-thermal components. The distribution of the thermal emission has been determined by analyzing H I, CO, and IRAS 60-μm data. We have found a good correlation between the 11-cm thermal continuum and the 60-μm emissions, which is used to obtain the thermal and non-thermal 11-cm continuum maps of the W51 complex.

Most of the thermal continuum is emanating from the compact H II regions and their low-density ionized envelopes in W51A and W51B. All the H II regions, except G49.1−0.4 in W51B, have associated molecular clumps. The thermal radio continuum fluxes of the compact H II regions are proportional to the CO fluxes of molecular clumps. This is consistent with the previous results that the total mass of stars in an H II region is proportional to the mass of the associated molecular clump.

According to our result, there are three non-thermal continuum sources in W51: G49.4−0.4 in W51A, a weak source close to G49.2−0.3 in W51B, and the shell source W51C. The non-thermal flux of G49.5−0.4 at 11-cm is ~28 Jy, which is ~25% of its total 11-cm flux. The radio continuum spectrum between 0.15 and 300 GHz also suggests an excess emission over thermal free-free emission. We show that the excess emission can be described as a non-thermal emission with a spectral index $\alpha \simeq -1.0$ ($S_\nu \propto \nu^\alpha$) attenuated by thermal free-free absorptions at low-frequencies. The non-thermal source close to G49.2−0.3 is weak (~9 Jy). The nature of the source is not known and the reality of the non-thermal emission needs to be confirmed. The non-thermal shell source W51C has a 11-cm flux of ~130 Jy and a spectral index $\alpha \simeq -0.26$.

Key Words: radio complex: W51, radio continuum: thermal and non-thermal,
ISM: H II regions, supernova remnants, molecular clouds

I. INTRODUCTION

In radio continuum, the Galaxy is pervaded by discrete sources immersed in a diffuse emission. The discrete sources, particularly the ones in the Galactic plane, usually appear to be superposed on the diffuse emission. Sometimes, several discrete sources happen to be superposed on each other in a small region. Probably the most extreme example of such a region is W51, an H II region complex located at the tangential point ($l = 49°$) of the Sagittarius arm (Bieging 1975; Mufson & Liszt 1979).

In single-dish radio continuum observations with a medium (~a few arcminutes) angular resolution, W51 appears to be composed of at least five compact sources and a large shell-like source, all embedded in a diffuse envelope (MACLEOD & Doherty 1968; Shaver 1969; Altenhoff *et al.* 1978). The compact sources are clustered

into two groups, W51A and W51B, separated by $\sim 20'$ along the Galactic plane (Kundu & Velusamy 1967). Figure 1a, which has been obtained from the Bonn 11-cm survey (Reich *et al.* 1990), shows the distribution of these sources in the W51 complex. In interferometric observations with a higher ($\lesssim 10''$) angular resolution, some of these compact sources break into several discrete sub-components (Martin 1972; Turner *et al.* 1974; Gaume, Johnston & Wilson 1993). Most, if not all, of the radio continuum emission associated with the compact sources are believed to be thermal. However, low-frequency observations seem to suggest a non-thermal component in some compact objects. For example, Wendker & Yang (1968) showed that the compact H II region G49.5−0.4 in W51A had an excess emission at $\nu \lesssim 3$ GHz which could be fitted by a spectral index $\alpha \simeq -0.8$ ($S_\nu \propto \nu^\alpha$). Salter *et al.* (1989) found an excess emission in one of the sub-components of G49.5−0.4 at $\nu < 5$ GHz by comparing their millimeter continuum fluxes with the centimeter continuum fluxes of Martin (1972). The large shell-like source W51C is probably a supernova remnant with its radio continuum being the non-thermal synchrotron emission (Kundu & Velusamy 1967; Mezger & Höglund 1967; Shaver 1969; Deshpande & Sastry 1986; Seward 1988; Copetti & Schmidt 1991). The nature of the diffuse envelope is not known.

The superposition of thermal and non-thermal sources and a diffuse emission makes it difficult to investigate the radio continuum properties of each individual source in the W51 complex. In this paper, we decompose the 11-cm continuum emission of the W51 complex into thermal and non-thermal components. We use the correlation between the radio continuum and the infrared brightness of H II regions. Both the radio continuum and the infrared emission from an H II region are proportional to the Lyman continuum luminosity of the central exciting source (e.g., Osterbrock 1989). A linear correlation between the two has been found for some H II regions (e.g., Harper & Low 1971; Fürst, Reich & Sofue 1987). For the W51 complex, the IRAS 60-μm image (Fig. 1b) shows that most of the 60-μm emission originates from two strong radio continuum sources W51A and W51B. Also, there is a diffuse infrared 'spur' extending to south from W51B, which suggests that the corresponding diffuse 11-cm continuum emission in Figure 1a is likely thermal. The shell-like source W51C does not appear in the 60-μm map. The similarity between the 11-cm continuum and the 60-μm maps suggests that we may use the correlation between the two to obtain the distribution of the non-thermal emission in the W51 complex. A similar technique has been applied by Broadbent, Haslam & Osborne (1989) to the 6-cm survey of Haynes *et al.* (1978) and to the 408-MHz survey of Haslam *et al.* (1982). They have identified new SNR candidates and have studied the radio continuum properties of the Galaxy. Our method differs from theirs in that we derive the 60-μm brightness associated with neutral gas by defolding the atomic and molecular gas distributions into separate galactocentric bins which have different infrared dust emissivities. Also, our H I data has a much higher angular resolution (3.3′) than theirs (36′).

We organize this paper as follows. In §2, we summarize the Arecibo H I 21-cm line observations, which yield the distribution of H I gas toward the W51 complex. In §3, we first derive the distributions of atomic and molecular gases toward the W51 complex at different Galactic radii. We then use the infrared emissivities derived by Bloemen, Deul & Thaddeus (1990) to compute the 60-μm surface brightness associated with neutral gas, which is subtracted from the IRAS 60-μm data to obtain the 60-μm emission associated with the ionized gas. Through the comparison with the 11-cm continuum map, we derive a correlation between the 60-μm and the 11-cm brightnesses of the ionized region. The correlation is used to obtain a 11-cm non-thermal map of the W51 complex. In §4, we analyze the resulting thermal and non-thermal maps, and compare them with previous results. We find a good correlation between the radio continuum fluxes of H II regions and the CO fluxes of associated molecular clumps. In §5, we discuss each individual source that appears in our non-thermal map. In §6, we summarize our results.

II. OBSERVATIONS

H I 21-cm line observations were carried out using the 305-m telescope (FWHM $\simeq 3'.3$) at the Arecibo Observatory[1] in 1991 September. Both circular polarizations were observed using two 1024-channel correlators, each with a total bandwidth of 5 MHz, so that the velocity resolution was 2.06 km s^{-1} (after Hanning smoothing). Each spectrum was obtained by integrating one minute using frequency switching. A rectangular area bounded by $\alpha_{1950} = (19^h18^m50^s - 19^h23^m06^s)$ and $\delta_{1950} = (13°36' - 14°30')$ has been mapped at 3′ spacing.

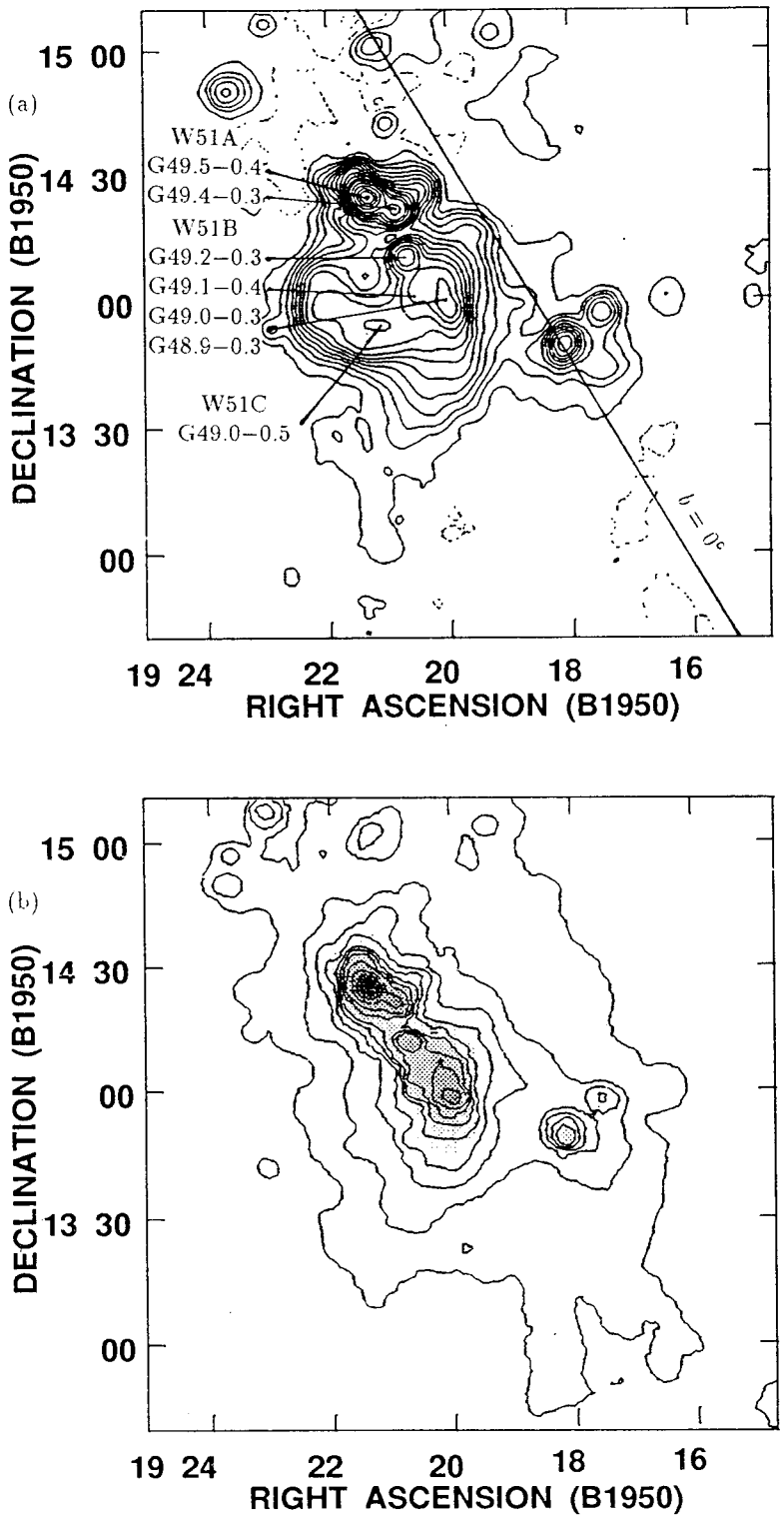

Fig. 1. (a) Distribution of the 11-cm radio continuum of the W51 complex. The 11-cm continuum map has been obtained from the Bonn survey (Reich *et al.* 1990). The median filter of $2.5° \times 10'$ has been applied to remove a smooth background. The contour levels are $T_b = -0.5$, -0.2, 0.2, 0.7, 1.2, 2, 3, 4.4, 6, 8, 11, 15, 22, 30, 45, 70, 100, 125 and 155 K. The negative contour levels are marked in dotted lines. The conventional name of each component is given. (b) Distribution of the IRAS 60-μm band emission toward the W51 complex. The contour levels are $I_{60} = 100$, 200, 400, 700, 1100, 1600, 2500, 4000, 7000, 10000 and 13000 MJy sr^{-1}. Grey-scale plot distinguishes hill from valley. (The higher flux-density is blacker.)

III. DECOMPOSITION OF THE 11-CM CONTINUUM EMISSION

1. Decomposition of the Infrared Emission

1) The Method

We first decompose the IRAS 60-μm intensity, I_{60}, toward the W51 complex into the components associated with neutral and ionized gases, $I_{60,n}$ and $I_{60,i}$. The distribution of $I_{60,n}$ may be obtained by applying the previously determined far-infrared (FIR) emissivity to the distribution of neutral gas. The FIR dust emissivity of neutral gas decreases rapidly with increasing galactocentric radius R, which is probably due to the variation of the general interstellar radiation field (Bloemen, Deul & Thaddeus 1990; Koo, Heiles & Reach 1992). In order to incorporate this variation, we follow Bloemen *et al.* (1990) to divide the path length along the W51 complex into four galactocentric bins[2] at radial intervals of $R=6.4\sim8.5$, $8.5\sim10.2$, $10.2\sim12.8$ and >12.8 kpc (column 1 of Table 1). The minimum galactocentric radius of the innermost bin corresponds to the tangential point along the W51 complex ($l=49°$). The 60-μm emissivity ε_{60}[MJy sr^{-1} (10^{20} H atom cm^{-2})$^{-1}$] of the dust mixed with atomic gas in each bin is listed in column 2 of Table 1 (Bloemen *et al.*). We assume that $I_{60,n}$ can be represented as a linear combination of the H I column density $N_{H\,I}$ and the velocity-integrated CO brightness temperature W_{CO} (K km s^{-1}) in these four bins:

$$I_{60,n}=\sum_{i=1}^{4}\varepsilon_{60,i}\,(N_{H\,I,i}+2\,Y_{60}\,W_{CO,i})+I_{60,b}, \tag{1}$$

where $I_{60,b}=0.39\pm0.08$ MJy sr^{-1} is an isotropic 60-μm background intensity, and $Y_{60}=(0.65\pm0.11)\times10^{20}$ molecules cm^{-2} (K km s^{-1})$^{-1}$ is the product of the conversion factor between W_{CO} and H_2 column density and the ratio of the infrared emissivity of the dust associated with molecular gas to that of atomic gas. Bloemen *et al.* found no evidence for a large-scale radial variation of Y_{60}.

The distributions of N_{HI} and W_{CO} are computed in the next section. Once we obtain an $I_{60,n}$ map from equation (1), then we may subtract it from the IRAS 60-μm map to obtain the distribution of the 60-μm emission associated with ionized gas.

Table 1. Properties of the 60-μm Dust Emission Associated with Neutral Gas.

Galactocentric Radius (Kpc)	ε_{60} (MJy sr^{-1} (10^{20} H atom cm^{-2})$^{-1}$)	$I_{60,HI}$ (MJy sr^{-1})	$I_{60,CO}$ (MJy sr^{-1})
$R_1=6.4\sim8.5$	0.51 ± 0.10	84.8	30.1
$R_2=8.5\sim10.2$	0.10 ± 0.02	0.8	0.2
$R_3=10.2\sim12.8$	0.12 ± 0.03	1.1	0.1
$R_4>12.8$	0.08 ± 0.02	0.7	0.0

2) Distribution of Neutral Gas

a. H I Column Density Distribution

The W51 complex is a strong radio continuum source near the tangential point. Therefore, in general, there are foreground and background H I gases that have the same line-of-sight velocity v_{LSR} (>0 km s^{-1}). H I 21-cm

[1]The Arecibo Observatory is a part of the National Astronomy and Ionosphere Center, which is operated by Cornell University under contact with the National Science Foundation.

[2]In this paper, we adopt the rotation curve of Clemens (1985) with $R_\odot=8.5$ kpc and $v_\odot=220$ km s^{-1}. We have scaled the radial intervals of Bloemen *et al.* (1990), who used $R_\odot=10$ kpc. Since the tangential point ($R\simeq6.4$ kpc) lies near the outer boundary of their second bin, we assume that the infrared emissivity in their third bin ($R=6.8\sim8.5$ kpc with $R_\odot=8.5$ kpc) is applicable up to the tangential point.

line is formed by (1) the H I emission from the foreground gas, (2) the continuum emission from the W51 complex attenuated by the foreground H I gas, and (3) the H I emission from the background gas attenuated by the foreground gas. The absorption of the continuum emission by the foreground H I gas can be seen in Figure 2a, which is the integrated H I brightness temperature map of the inner solar circle ($v_{LSR}>0$ km s^{-1}). In Figure 2a, we can see a strong absorption toward W51A and relatively weak absorptions toward W51B and W51C. The corresponding map of the outer solar circle ($v_{LSR}<0$ km s^{-1}) is shown in Figure 2b. The weak absorption-like features toward W51A and W51C in Figure 2b are not likely due to the absorption, but probably due to the distribution of the H I gas in the outer galaxy.

In order to compute the H I column density distribution, we consider a simple model where, at a given v_{LSR} (>0 km s^{-1}), two H I clouds of optical depth $\tau_1(v)$ (closer one) and $\tau_2(v)$ (farther one) are located symmetrically with respect to the tangential point. The W51 complex is assumed to be located between two clouds. We further assume that the H I clouds have the same spin temperature $T_s=160$ K, which corresponds to the maximum brightness temperature in this region. We use the main beam efficiency of 0.84 to convert the observed antenna temperature to the brightness temperature. In this model, the observed H I 21-cm brightness temperature profile $T_{obs}(v)$ is given by

$$T_{obs}(v)=T_s[1-e^{-\tau(v)}]-T_c[1-e^{-\tau_1(v)}], \tag{2}$$

where T_c is the continuum brightness temperature of the W51 complex and

$$\tau(v)=\tau_1(v)+\tau_2(v). \tag{3}$$

If $T_c \ll T_s$, then we obtain $\tau(v)$ from equation (2), which yields the H I column density:

$$N_{HI}=1.823\times10^{18}T_s\int\tau(v)dv \qquad (\text{cm}^{-2}). \tag{4}$$

The H I column densities due to the gas at $v_{LSR}<0$ km s^{-1}, i.e., in the outer solar circle, can be computed straightforwardly from the above equations, i.e., $T_c=0$ in equation (2). At $v_{LSR}>0$ km s^{-1}, we first compute the H I column densities assuming $T_c=0$. Then we compare the computed with the observed variations of $N_{H\,I}$ along slices connecting the upper-left corner of Figure 2a and the other ends of the map. These one-dimensional plots, which have reasonable 'baselines', reveal the regions affected by absorption. The H I column densities in those absorption-affected regions are smoothly interpolated using the above one-dimensional plots.

Toward the continuum peaks of W51A, W51B, and W51C, where we see obvious absorptions in Figure 2a, we may separate the observed profiles into the emissions from the foreground and background gases. The 'expected' profiles toward these sources, $T_{exp}(v)$, which are free from absorptions, are generated from surrounding profiles. For G49.5−0.4 (W51A) and G49.2−0.3 (W51B), the expected profiles are generated by averaging two profiles separated by $\pm12'$ along RA axis from them. For G49.0−0.5 (W51C), the expected profile is generated by averaging two profiles, one at 12′ south and the other at 18′ east from it. Figure 3 (bottom pictures) compares the expected profiles (dotted lines) with the observed profiles (solid lines). The difference between the observed and the expected profiles is proportional to $T_c[1-e^{-\tau_1(v)}]$. If we know T_c, we can determine $\tau_1(v)$ and therefore the H I column density of foreground gas. The 21-cm brightness temperatures of the continuum peaks have been obtained by scaling the 11-cm Bonn survey, which has a beam size similar to the H I data. The spectral slopes have been computed by comparing the 11-cm map convolved with the beam of the 21-cm Bonn survey (FWHM$\simeq$8.′4) and the brightness temperature in the 21-cm Bonn survey (Reich, Reich & Fürst 1990). The computed spectral slopes are $\alpha\simeq+0.3$, -0.1, and -0.2, and the 21-cm brightness temperatures are $T_c\simeq464$, 143, and 64K, for G49.5−0.4, G49.2−0.3, and G49.0−0.5, respectively. The resulting profiles due to the foreground (solid lines) and background (dotted lines) gases are shown in Figure 3 (top pictures). The negative dips in the resulting profiles are due to an error in generating the expected profiles. Also the foreground emission at negative velocities, particularlly in G49.0−0.5, are due to an error in the expected profiles. Table 2 shows the computed foreground, background, and the total H I column densities

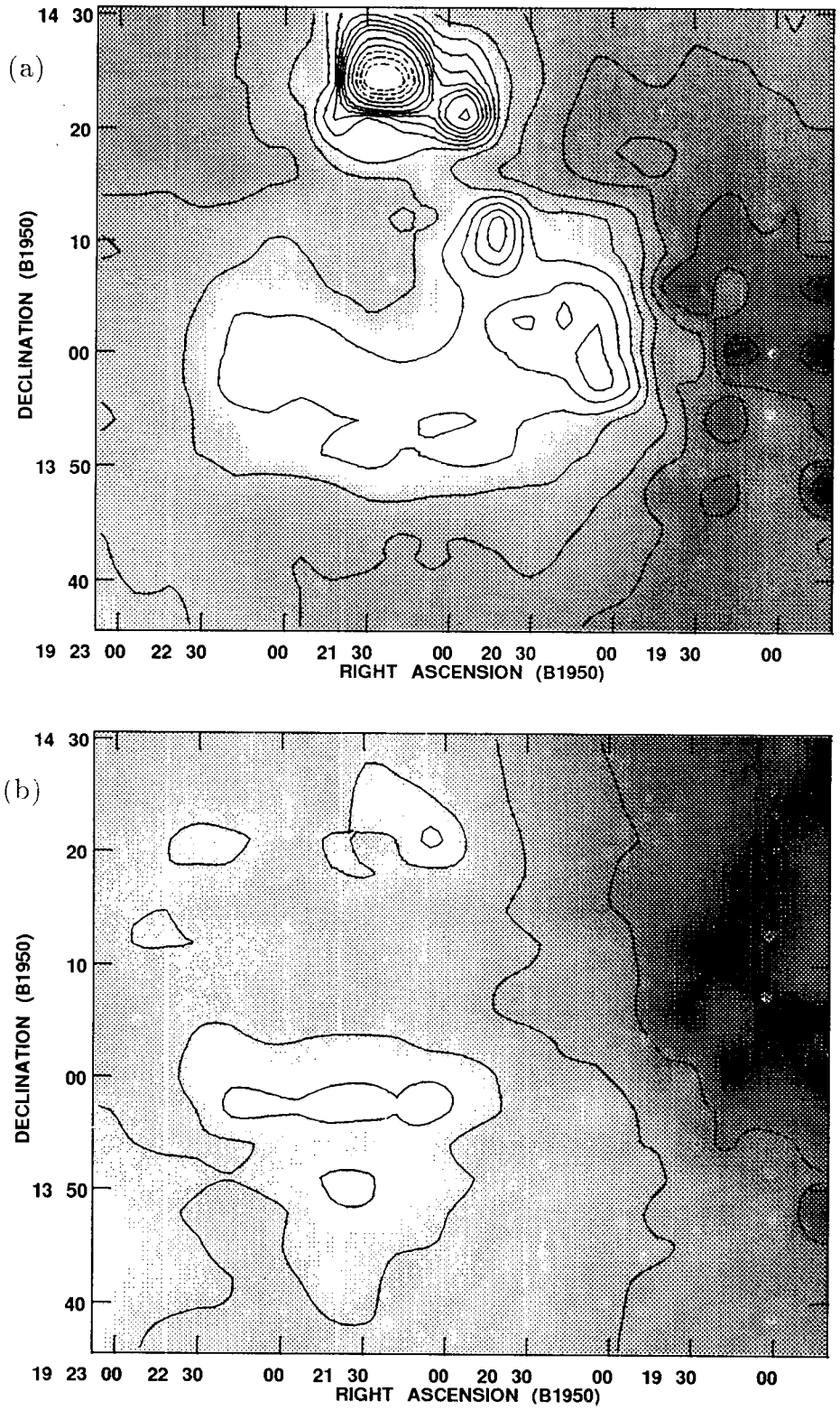

Fig. 2. (a) Distribution of the integrated H I emission between $v_{LSR}=0$ and $+250$ km s^{-1} toward the W51 complex. The continuum sources in Figure 1a appear in absorption against the background emission. The lowest contour level is $\int T_b(v)dv=-3\times10^3$ K km s^{-1}. The levels increase by 1×10^3 to 2×10^3. The next two levels are 4520 and 5000 and then the levels increase by 500 to 7500. (b) Same as (a) but between $v_{LSR}=-250$ and 0 km s^{-1}. The contour levels are $\int T_b(v)dv=0.95$, 1.05, 1.3 and 1.7×10^3 K km s^{-1}.

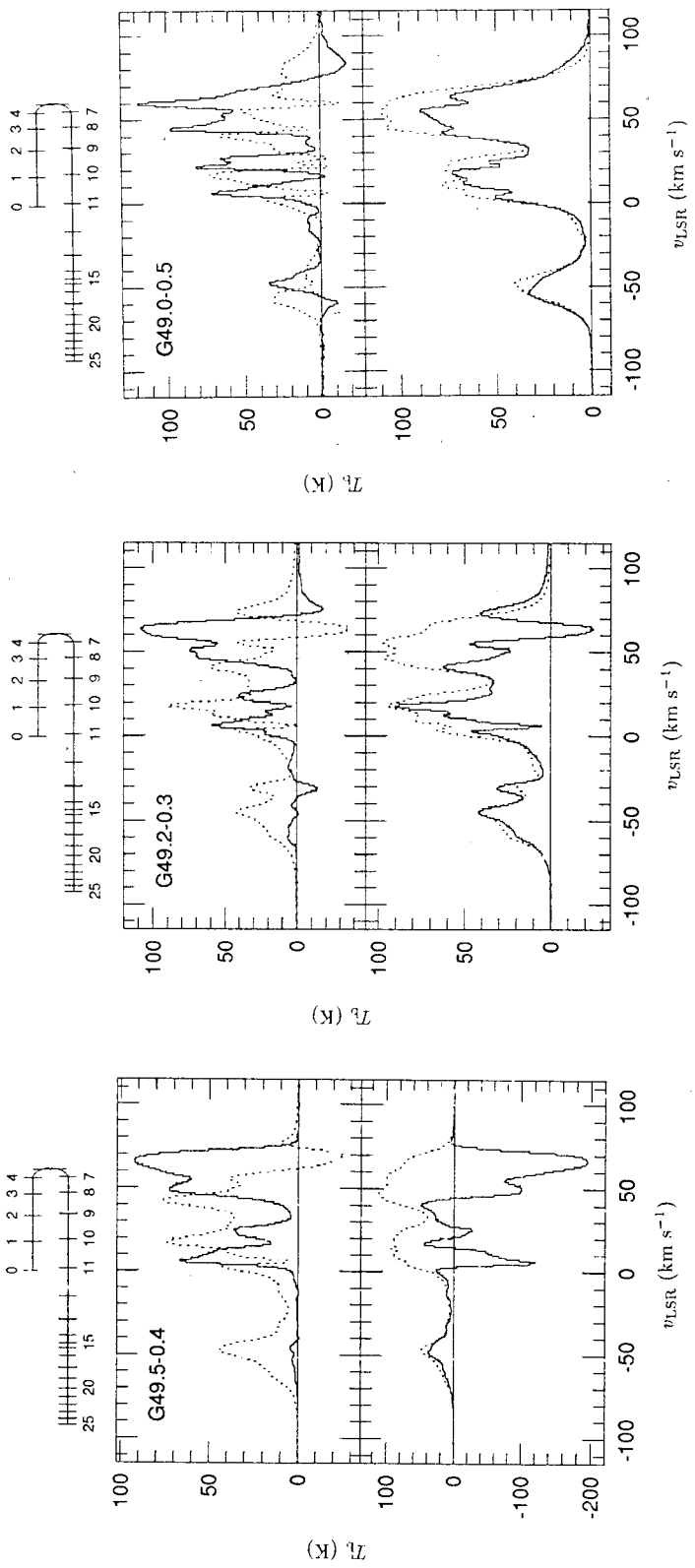

Fig. 3. (bottom pictures) Observed (solid line) and expected (dotted line) H I 21-cm profiles toward strong continuum sources in the W51 complex. (top pictures) Computed H I 21-cm emission profiles from the foreground (solid line) and background (dotted line) gases. See text for explanations. At the top of the figure is a curve that shows the relation between velocity and distance from the Sun (in kpc) for an Galactic rotation curve of Clemens (1985).

toward each source. According to Table 2, the amounts of H I gas in the foreground and the background are comparable toward these sources; the H I column densities in both sides are in the range of $N_{H\,I}=(7\sim10)\times10^{21}$ cm^{-2}. We have obtained similar results toward other compact sources in W51A and W51B, which are not shown in Figure 3.

Table 2. H I Column Densities toward the Strong Continuum Sources.

Name	Foreground Column Density (cm^{-2})	Background Column Density (cm^{-2})	Total Column Density (cm^{-2})
G49.5−0.4	7.6×10^{21}	9.7×10^{21}	1.7×10^{22}
G49.2−0.3	7.0×10^{21}	8.7×10^{21}	1.6×10^{22}
G49.0−0.5	8.4×10^{21}	8.5×10^{21}	1.7×10^{22}

b. CO Integrated Intensity Distribution

We use the ^{12}CO data of Massachusetts-Stony Brook Galactic plane survey (HPBW=50″, Sanders *et al.* 1986) to compute the integrated ^{12}CO intensity W_{CO}. The ^{12}CO data was sampled coarsely, at every 3′, and we simply interpolate in bicubic the observed integrated intensities to obtain the W_{CO} distribution. The main beam efficiency of 0.75 is used to convert the observed chopper wheel antenna temperature to the brightness temperature (Sanders *et al.* 1986). Figure 4 shows the distribution of the total integrated CO intensity, where we see strong CO emissions associated with W51A and W51B.

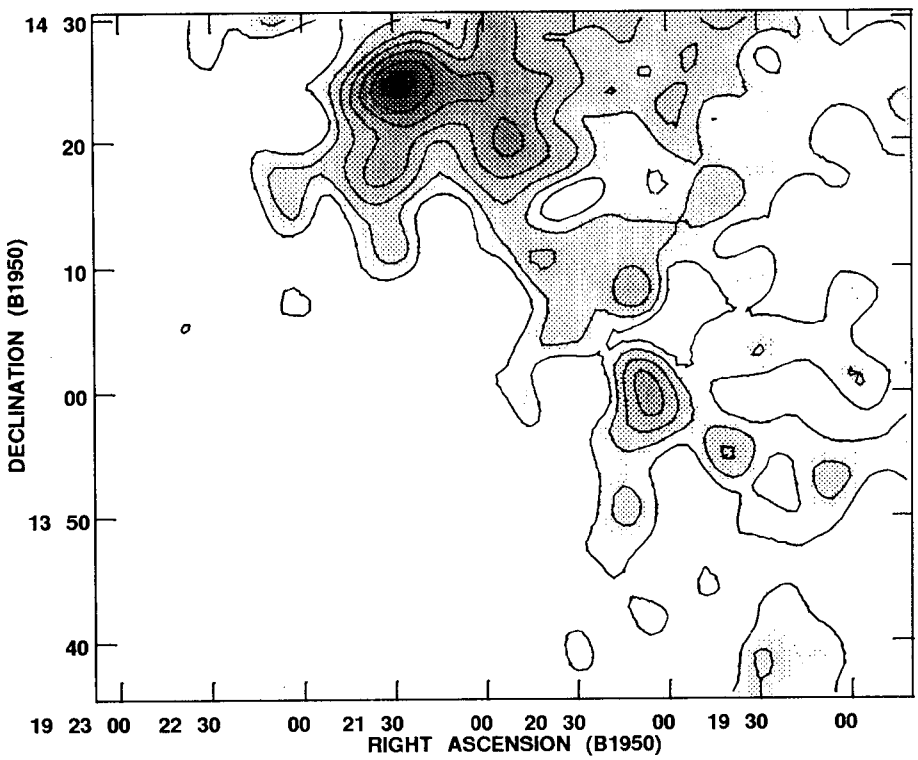

Fig. 4. Distribution of the integrated ^{12}CO J=1−0 emission between $v_{LSR}=-100$ and +100 km s^{-1} toward the W51 complex. The contour levels are $\int T_b(v)dv=60$, 90, 130, 180, 240, 310, and 390 K km s^{-1}.

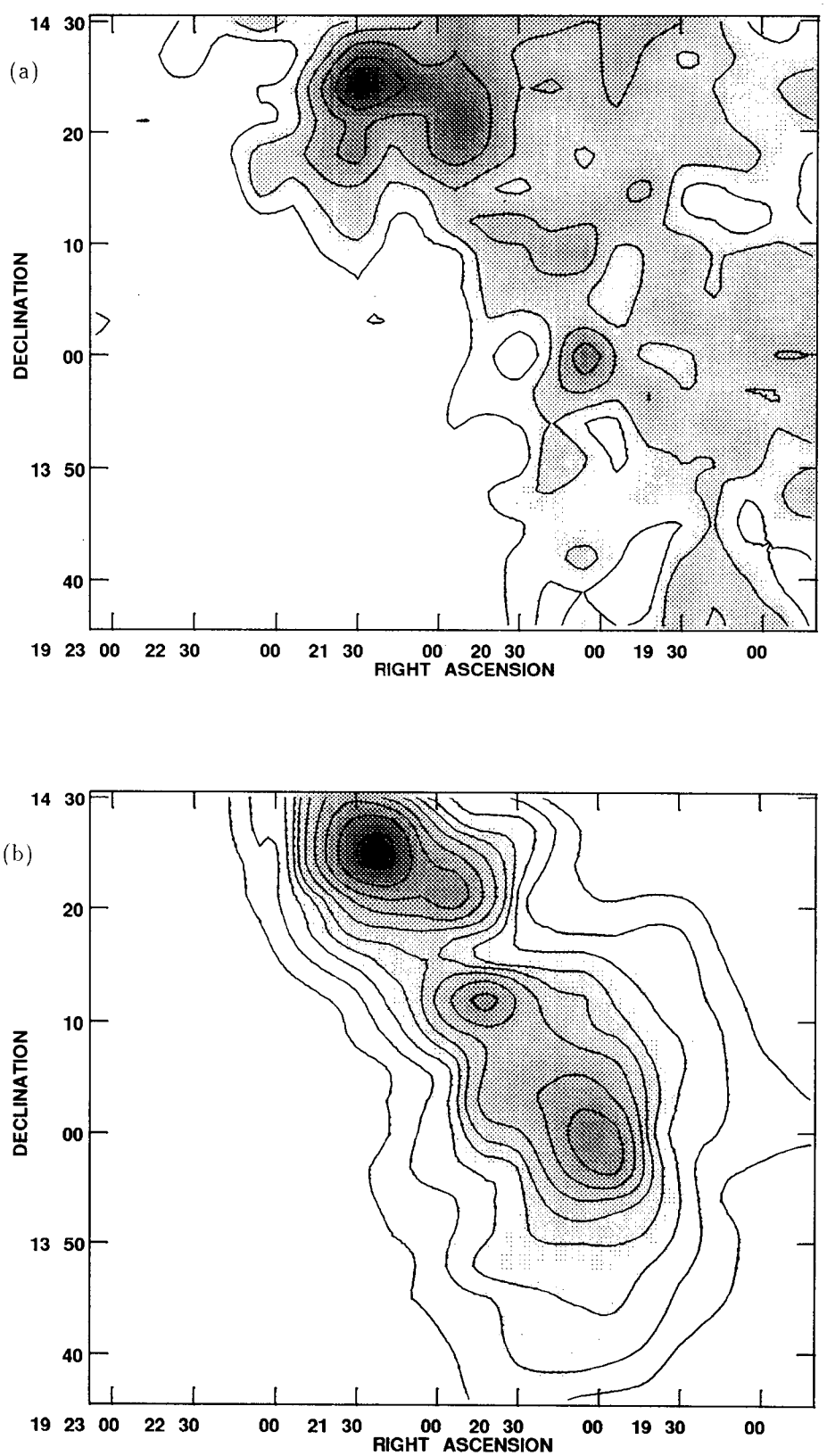

Fig. 5. (a) Distribution of the IRAS 60-μm band emission from the dusts associated with the neutral gas toward the W51 complex. The contour levels are $I_{60,n}=110$, 130, 160, 200, 250 and 310 MJy sr^{-1}. (b) Same as (a) but from the dusts associated with the ionized gas. The contour levels are $I_{60,i}=200$, 400, 700, 1100, 1600, 2500, 6000, 9000 and 13000 MJy sr^{-1}.

3) Infrared Emissions Associated with Neutral and Ionized Gases

The derived $N_{H\,I}$ and W_{CO} distributions in each bin are substituted into equation (1) to compute the distribution of the 60-μm intensity associated with neutral gas (Figure 5a). Toward the W51 complex, we have found that the mean 60-μm intensities associated with atomic and molecular gas, $I_{60,HI}$ and $I_{60,CO}$, are 87 and 31MJy sr^{-1}, respectively. The maximum of $I_{60,HI}$ (140 MJy sr^{-1}) occurs near the western boundary of the map, whereas the maximum of $I_{60,CO}$ (230 MJy sr^{-1}) occurs toward G49.5−0.4. Most (97%) of the 60-μm emission associated with neutral gas originates from the inner solar circle. The contribution from each bin is listed in columns 3 and 4 of Table 1.

By subtracting the $I_{60,n}$ map from the IRAS 60-μm map, we obtain the distribution of the 60-μm intensity associated with ionized gas, $I_{60,i}=I_{60}-I_{60,n}$ (Figure 5b). According to Figure 5, about 87% of the 60-μm flux originates from the dusts associated with ionized gas, whereas 9% and 4% are from the dusts associated with atomic and molecular gases. These values are very different from the Galactic averaged values. Broadbent *et al.* (1989) deduced that, in the inner Galaxy, about 42% of the 60-μm emission is H II-associated and 58% is H I-associated. Therefore, toward the W51 complex, the dust emission from ionized component is dominant, and the molecular component cannot be neglected compared to the atomic component.

2. Thermal and Non-Thermal Radio Continuum Emissions

Figure 6a shows the correlation between the 11-cm brightness temperature T_{11} (K) and the *total* 60-μm intensity I_{60} (MJy sr^{-1}) in the W51 complex region. The 11-cm radio continuum data was sampled at 2′ spacing with a beam size of FWHM$\simeq$4.2′. In order for comparison, we have resampled the data at 3′ spacing with a gaussian beam of FWHM=3′. We see a rough linear correlation between T_{11} and I_{60}, if we exclude the pixels toward W51C (empty-circles). But at $T_{11}\lesssim 1$ K, the 60-μm intensity saturates to $\sim$100 MJy sr^{-1}. This saturation is due to the 60-μm emission associated with neutral gas. Figure 6b shows the correlation between T_{11} and the 60-μm emission associated with the *ionized* gas. We see a significant improvement in the correlation (correlation coefficient of 0.94), particularlly at $T_{11}\lesssim 1$ K. The linear correlation now extends to very low surface brightnesses although the scatter gets larger. The pixels toward W51C generally have an excess 11-cm continuum emission, which is presumably due to the non-thermal emission.

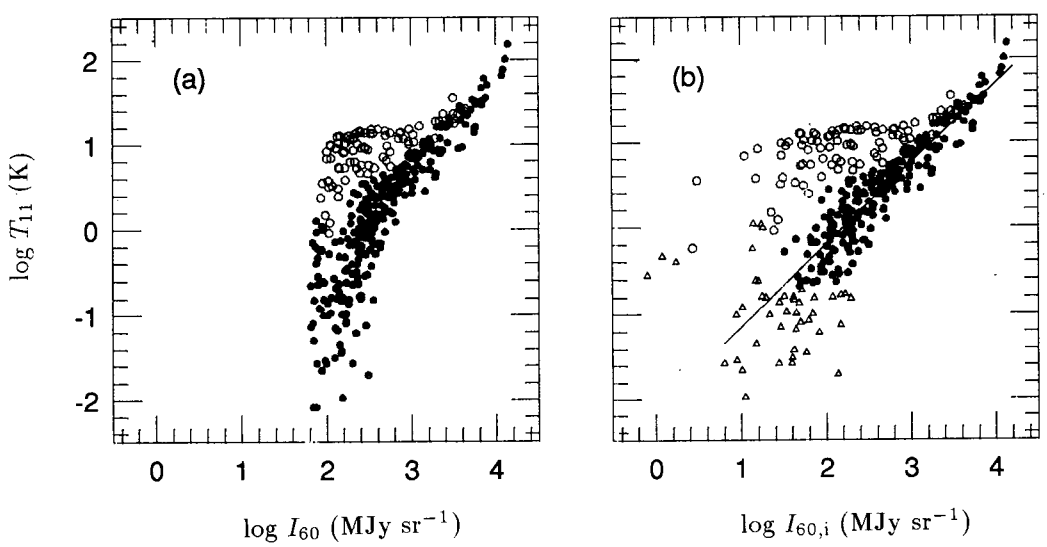

Fig. 6. (a) Comparison of the 11-cm continuum brightness temperature T_{11} with the total 60-μm intensity I_{60}. Empty-circles represent pixels toward W51C. A rough correlation between the two can be seen. At $T_{11}\lesssim 1$ K, I_{60} saturates to $\sim$100 MJy sr^{-1}. (b) Same as (a) but with the 60-μm intensity from the dusts associated with ionized gas $I_{60,i}$. The correlation has been improved significantly. The solid line is a least-square fit (eq. 5 in text). Empty-triangles represent pixels of noisy level excluded in fitting.

In order to derive the correlation between the 11-cm *thermal* brightness temperature $T_{11,th}$ and $I_{60,i}$, we exclude those pixels toward W51C and the pixels with $T_{11}<0.2$ K or $I_{60,i}<24$ MJy sr^{-1} (empty-triangles) which corresponds to 1σ of the 11-cm background fluctuation. A least-square fit yields

$$T_{11,th}=(7.9^{+2.1}_{1.6})\times 10^{-3} I_{60,i}. \quad (5)$$

The coefficient in equation (5) is comparable to the average value in the Galactic plane, $(6.4\pm1.7)\times10^{-3}$, derived by Broadbent *et al.* (1989).

We may apply equation (5) to Figure 5b in order to obtain a thermal 11-cm continuum map of the W51 complex. By subtracting the thermal contributions from the 11-cm map, we obtain the *non-thermal* 11-cm continuum map of the W51 complex. Figures 7a and 7b show the resulting thermal and non-thermal maps. The 1σ error of each pixel in Figures 7a and 7b due to the uncertainty in the derived correlation (eq. 5) is $\sim$20% of its total brightness temperature.

IV. SOME GENERAL PROPERTIES

1. Thermal Emission and Molecular Clouds

Figure 7a shows that the thermal emission is composed of compact H II regions superposed on diffuse emission. The peak brightness temperatures and the fluxes of compact sources derived from Figure 7a are listed in columns 2 and 3 of Table 3. The fluxes of compact sources are derived by two-dimensional elliptical gaussian fittings. According to Table 3, total 11-cm flux due to the compact H II regions is $\sim$220 Jy, which is $\sim$65% of the total 11-cm thermal flux. There are several points to be made from Figure 7a. First, the brightness of the compact H II region G49.5$-$0.4 in W51A has decreased considerably. The thermal flux is about 75% of the total 11-cm flux. The remaining 25% has turned out to be non-thermal (see §5.1). Second, there is a diffuse emission extending to south from W51B. This radio 'spur' is almost vertical to the Galactic plane. If we adopt 5 kpc, the distance to W51B (Wilson *et al.* 1970; Bieging 1975; Mufson & Liszt 1979), as the distance to the spur, the linear size is $\sim$40 pc. The association of the spur with the compact H II regions in W51B needs to be studied.

Table 3. Parameters of Compact H II Regions and Associated Molecular Clumps.

Name	T_{peak} (K)	$S_{11,th}$ (Jy)	v_{RRL} (km s^{-1})	F_{CO} (K km s^{-1}sr)	M_c ($M_\odot$)	M_* ($M_\odot$)
G49.5$-$0.4	64	80$\pm$24	55$\sim$67	9.9×10^{-4}	1.2×10^5	3.0×10^4
G49.4$-$0.3	42	34$\pm$10	48$\sim$59	5.4×10^{-4}	9.8×10^4	1.9×10^4
G49.2$-$0.3	28	26$\pm$ 8	54$\sim$71	1.5×10^{-4}	1.4×10^4	1.0×10^4
G49.0$-$0.3[1]	32	78$\pm$23	62$\sim$71	6.6×10^{-4}	6.1×10^4	1.9×10^4

[1]Superposed on G48.9$-$0.3.

By comparing Figure 7a with Figure 4, we find that the compact H II regions in W51A and W51B are closely associated with molecular clouds. The association is more clearly seen in Figure 8, which is the (l, v) diagram of the ^{12}CO emission. The positions and velocities of the compact H II regions are marked by error bars. The velocities are those of radio recombination lines (column 4 of Table 3) from previous observations (Reifenstein *et al.* 1970; Wilson *et al.* 1970; Gordon, Gordon & Lockman 1974; Mufson & Liszt 1979; Pankonin, Payne & Terzian 1979; Wilson, Bieging & Wilson 1979; Garay, Reid & Moran 1985). Figure 8 shows that all the compact H II regions, except G49.1$-$0.4 in W51B, are located close to the local peaks of CO emission, which implies that these H II regions are still embedded in their parental molecular clouds.

The association of H II regions with molecular clouds in the Galaxy has been studied previously (Myers *et al.* 1986; Waller *et al.* 1987; Scovill *et al.* 1987; Wood & Churchwell 1989). Myers *et al.* have found that the

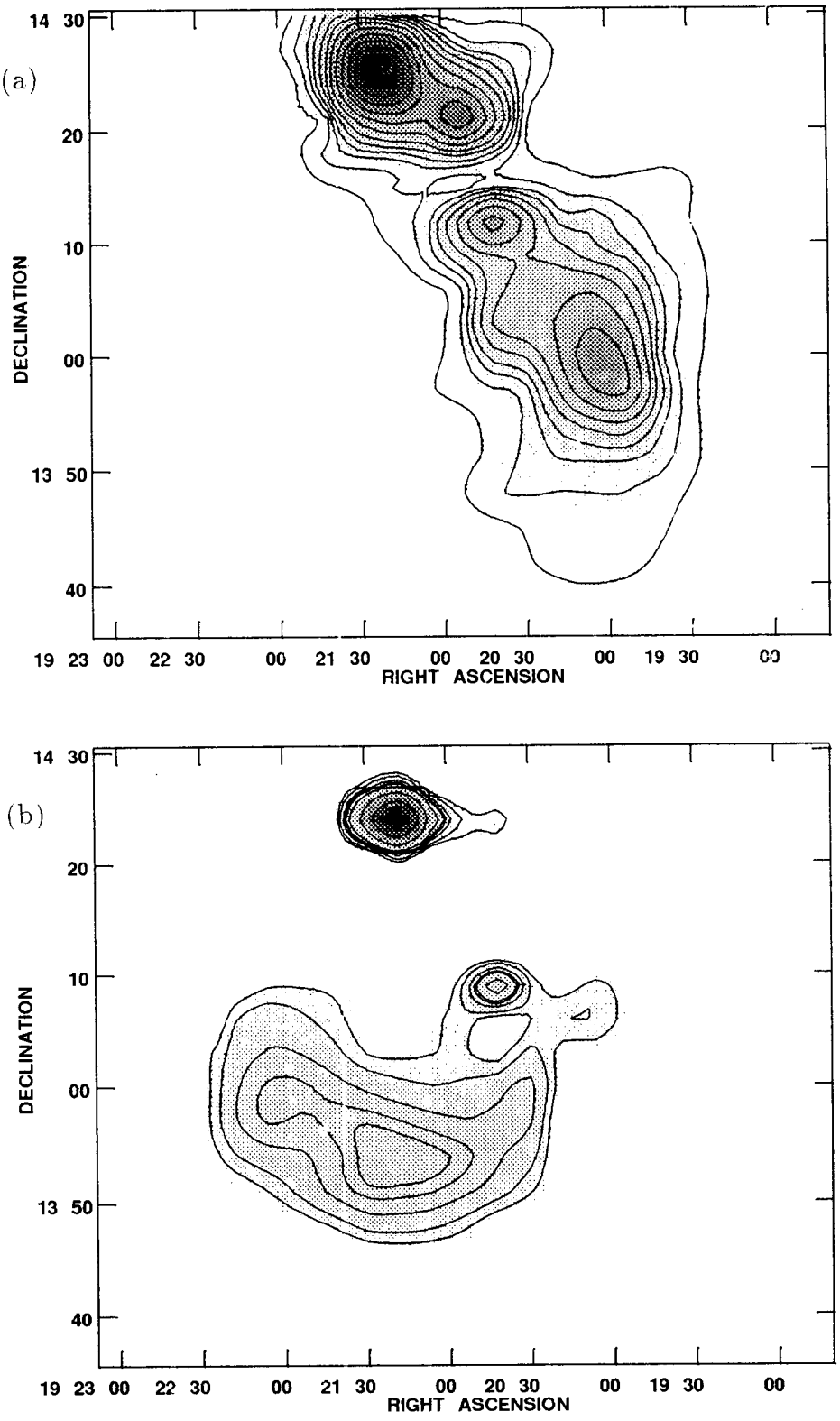

Fig. 7. (a) Distribution of the 11-cm thermal continuum of the W51 complex. Most of the emission is emanating from the compact H II regions and their ionized envelopes in W51A and W51B. The contour levels are T_b=1, 3, 5, 7, 9, 12, 16, 22, 30, 40, 50, 60 and 70 K. The grey-scale varies from 1 to 80 K. (b) Distribution of the 11-cm non-thermal continuum of the W51 complex. There are three non-thermal sources. A strong source at G49.5−0.4, a weak source close to G49.2−0.3, and the shell source W51C. The contour levels are T_b=5, 7, 10, 12, 13, 17, 30, 50, and 80 K. The grey-scale also varies from 1 to 80 K.

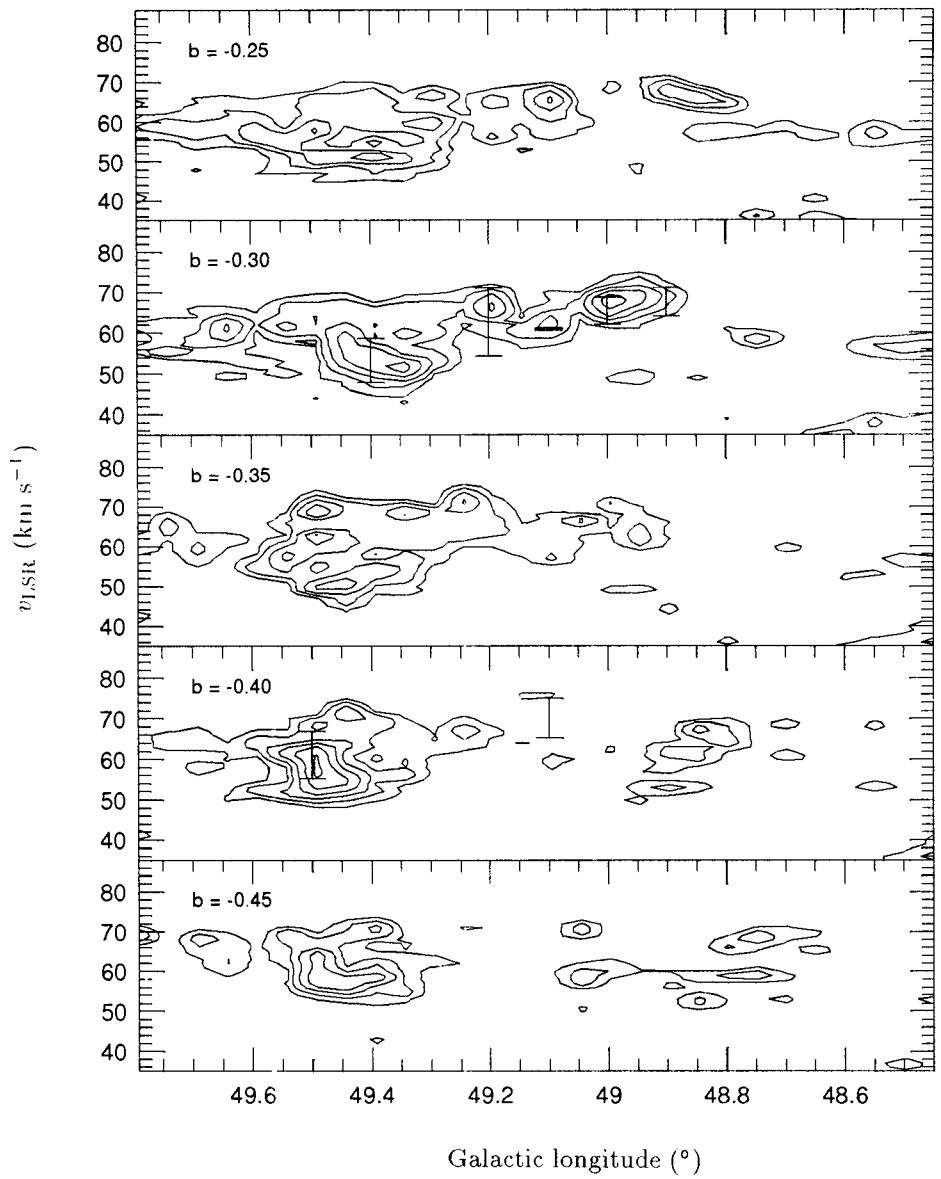

Fig. 8. The Galactic longitude-velocity (l, v) diagrams of ^{12}CO J=1−0 emission at Galactic latitude $b=-0.25°$, $-0.30°$, $-0.35°$, $-0.40°$ and $-0.45°$. The error bars represent the positions and velocities of compact H II regions in the W51 complex. The contour levels are T_b=2.6, 5.2, 9.1, 14.3, 20.8, and 28.9 K.

mass of stars in H II region M_* estimated from radio continuum flux (and FIR flux) is proportional to the mass of associated molecular cloud M_c: $M_*=(20^{+80}_{-16})\ M_c^{0.5\pm0.2}$ where M_* and M_c are in solar masses. We explore the similar relationship in the W51 complex.

We compare the 11-cm thermal continuum fluxes $S_{11,th}$ (Jy) of H II regions with the CO J=1−0 fluxes $F_{CO}=\int\int T_b\ dvd\Omega$ (K km s^{-1}sr) of associated dense molecular clumps. Figure 8 shows that dense molecular clumps are embedded in a diffuse interclump gas. In order to derive F_{CO}, the velocity intervals and the RA and DEC boundaries of each clump are determined in position-velocity diagrams, and the CO emission in a data cube has been integrated. The derived CO fluxes are listed in column 5 of Table 3. Figure 9 shows that $S_{11,th}$ and F_{CO} are correlated (correlation coefficient of 0.87). Note that there is no distance effect in Figure 9. A least-square fit yields

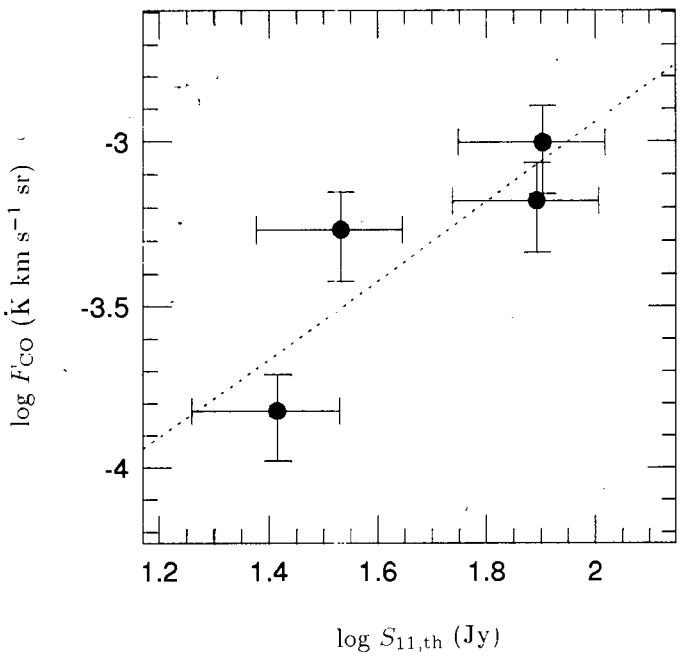

Fig. 9. Comparison between thermal 11-cm fluxes of compact H II regions in the W51 complex and CO fluxes of associated dense molecular clumps. The dotted line is a least-square fit (eq. 6 in text).

$$F_{CO}=(4.0^{+28}_{-3.5})\times 10^{-6}\ S_{11,th}^{1.2\pm 0.5}, \tag{6}$$

which is shown as a dotted line in Figure 9.

The correlation given by eq. (6) implies that the thermal continuum flux of a H II region is proportional to the mass of the associated molecular clump, $M_c \propto F_{CO}$. If we use the conversion ratio $N_{H_2}/W_{CO}=2.3\times 10^{20}$ molecules cm^{-2} (K km s^{-1})$^{-1}$ (Strong *et al.* 1988) where again W_{CO} is the integrated CO intensity and N_{H_2} is the H_2 column density, the mass of molecular clump is given by $M_c \simeq 3.7\times 10^6\ F_{CO}\ d^2$, where d is the distance to source in kpc. We use $d=7$ kpc for W51A (G49.5−0.4 and G49.4−0.3) (Genzel *et al.* 1981; Schneps *et al.* 1981) and $d=5$ kpc for W51B (G49.2−0.3 and G49.0−0.3). The derived masses of molecular clumps are listed in column 6 of Table 3. Their masses, $10^4 \sim 10^5\ M_\odot$, are typical values of giant molecular clouds (Goldsmith 1987). In order to derive the total mass of stars, in each H II region, we follow Myers *et al.* (1986). We first calculate the Lyman-alpha (Lyα) luminosity from the 11-cm thermal flux by assuming an electron temperature of 7,000K. The Lyα luminosity may be used to derive the total mass for a given initial mass function (Ho & Haschick 1981). We use the initial mass function of Miller & Scalo (1979). (See Myers *et al.* for a detailed explanation.) The resulting stellar masses of H II regions are listed in column 7 of Table 3. According to Table 3, the stellar masses are related to masses of molecular clumps by $M_*=(160^{+340}_{-110})\ M_c^{0.4\pm 0.1}$. The power-index 0.4 is comparable to that of Myers *et al.* (1986). However, the coefficient ~160 is much larger than ~20 of Myers *et al.*. The difference is partly due to the different approach in estimating the mass of associated molecular cloud and also partly due to the large star-formation-efficiency (SFE) of the W51 complex (see next).

We also compare the total 11-cm thermal flux and the total mass of molecular gas in W51A and W51B, both including diffuse emission (Table 4). In Table 4, columns 2, 3, and 4 contain the 11-cm thermal flux, the mass of molecular gas, and total stellar mass of W51A and W51B, respectively. The SFE, which is defined as the ratio of the stellar mass to the total mass (Myers *et al.* 1986) may be computed from M_* and M_c, and they are listed in column 5 of Table 4. According to Table 4, the SFE is 0.06 and 0.16 for W51A and W51B, respectively. These values are considerably larger than the average value 0.02 for $12° < l < 60°$ and also larger than 0.04 of the W51 giant molecular complex as a whole (Myers *et al.* 1986). The large SFEs suggest that the

W51 complex is one of the most active star-forming regions in the Galaxy. The relatively large SFE of W51B may suggest that W51B is in a more evolved stage of star formation compared to W51A. This is consistent with the absence of usual indicators of current star formation such as OH and H_2O maser sources and near infrared sources in W51B (Pankonin *et al.* 1979).

Table 4. Global Properties of W51A and W51B.

Name	$S_{11,th}$ (Jy)	M_c ($M_\odot$)	M_* ($M_\odot$)	SFE
W51A	160±20	1.0×10^6	6.0×10^4	0.06
W51B	180±25	2.0×10^5	3.8×10^3	0.16

2. Non-Thermal Emission

According to Figure 7b, the *non-thermal* 11-cm continuum emission of the W51 complex is composed of three sources: (a) a strong compact source at G49.5−0.4 in W51A, (b) a weak compact source close to G49.2−0.3 in W51B, and (c) the extended shell source W51C. There are weak emissions at G49.4−0.3 in W51A and (α_{1950}, δ_{1950})≃($19^h20^m12^s$, 14°05′56″) in W51B. They are, however, not significant because their peak intensities are comparable to the 1σ error level. The 11-cm non-thermal emission constitutes ~35% of the total 11-cm flux. The peak position, the 11-cm peak brightness temperature, and flux of each source, derived from Figure 7b, are listed in columns 2, 3, and 4 of Table 5. The shell source W51C has been known to be non-thermal from previous studies, whereas the other two compact sources have not. Particularly, the strong peak at G49.5−0.4 is surprising because it has been known as an H II region.

Table 5. Parameters of the 11-cm Non-thermal Continuum Sources.

Name	Peak Position (α_{1950}, δ_{1950})	T_{peak} (K)	$S_{11,nth}$ (Jy)
G49.5−0.4	($19^h21^m18^s$, 14°23′59″)	83.2	28±15
W51B[1]	($19^h20^m42^s$, 14°08′57″)	19.9	9±4
W51C	($19^h21^m18^s$, 13°53′59″)	13.8	133±40

[1]Unidentified source close to G49.2−0.3.

Figure 7b may be compared with the 151 MHz aperture synthesis map (FWHM≃2×5 arcmin^2) of Copetti & Schmidt (1991). Although Copetti & Schmidt have not decomposed the 151 MHz emission into thermal and non-thermal components, the comparisons might be useful because the frequency is low enough for the non-thermal emission to be dominant. In their 151 MHz map, G49.5−0.4 is no more the strongest source. In fact, its flux ~17 Jy is much smaller than either 80±12 Jy of G49.2−0.3 (in their 151 MHz map, labeled as G49.2−0.4) in W51B or the fluxes of local maxima in W51C, 62±9 Jy of G49.0−0.5 and 52±8 Jy of G49.2−0.7. The relatively large decrease in the W51A's flux is because its continuum emission becomes optically thick at $\nu<$ 1 GHz (Shaver 1969; Copetti & Schmidt 1991; see also §5.1). In the 151 MHz map, G49.2−0.3 is the brightest in the W51 complex. The 11-cm weak compact source in Figure 7b is located at ~3′ toward the south of the 151 MHz peak. If we use the 151 MHz flux and our 2.7 GHz thermal flux of G49.2−0.3, we obtain the spectral index $\alpha\simeq-0.3$ which is considerably different from thermal emission. Therefore, there could be a significant non-thermal contribution at 151 MHz, which may be associated with the weak compact source in Figure 7b. In the 151 MHz map, W51C clearly appears as an incomplete shell of ~30′ diameter with its northern portion opened. There are two local maxima, G49.5−0.5 and G49.2−0.7. In Figure 7b, we also see an incomplete shell W51C with two local maxima, although they are slightly smoothed out due to our large beam size.

V. INDIVIDUAL SOURCES

1. G49.5−0.4

According to our result, about 25% of the 11-cm flux of G49.5−0.4 is non-thermal. This is surprising because G49.5−0.4 is an H II region complex (Martin 1972). The peak brightness temperature of the non-thermal emission is 83 K, which is greater than 74 K of the thermal emission. It is possible that the thermal radio continuum from G49.5−0.4 is considerably stronger than what we would expect from eq. (5). In that case, the non-thermal emission of G49.5−0.4 in Figure 7b could be due to an error associated with our thermal and non-thermal and non-thermal decomposition method. However, there have been suggestions for a non-thermal component in G49.5−0.4 from radio studies, too. Wendker & Yang (1968) noted that the radio spectrum of G49.5−0.4 between 0.2 and 15 GHz could not be described by a single spectral index. Instead, it could be fitted by an optically-thin thermal free-free emission with a spectral index $\alpha=-0.1$ plus an excess emission with $\alpha=-0.8$. The excess emission has a flux of ~30 Jy at 2.7 GHz, which is comparable to our result. On the other hand, Salter et al. (1989) suggested that one of the sub-components of G49.5−0.4, W51b, had a non-thermal component. The non-thermal flux of W51b, ~4 Jy at 2.7 GHz, however, is small compared to the total excess flux, ~30 Jy, of G49.5−0.4. Hence, the presence of a non-thermal component toward G49.5−0.4 in Figure 7b, which has been obtained from a completely different approach, seems to be consistent with these radio studies.

Table 6 summarizes previous observational results on G49.5−0.4 between 0.15 and 300 GHz. Columns (1) and (2) contain the central frequency and the angular resolution of each observation. Columns (3), (4), and (5) contain the size, flux-density, and its error obtained by each observation, respectively. At frequencies above ~100 GHz, thermal emission from dust grains becomes important (Salter *et al.* 1989). The flux-densities at $\nu\geq 140$ GHz in Table 6 is from Sievers *et al.* (1991), where the contamination of dust emission has been removed. Column (6) contains the reference for each observation. Figure 10a shows the flux-density distribution of G49.5−0.4 in Table 6 (empty-circles). In Figure 10a, we see that the emission has a turn-over at $\nu_c\sim 2$ GHz. At $\nu>\nu_c$, the spectral index is $\alpha\simeq -0.18$, whereas at $\nu<\nu_c$, it is $\alpha\simeq 0.82$. These indices are considerably different from $\alpha=-0.1$ and $+2.0$ of thermal free-free emission in optically-thin and optically-thick cases, respectively.

The large departure of spectral indices and the presence of a strong peak in our non-thermal map lead us to investigate radio continuum emission from G49.5−0.4 in detail. We decompose the flux-density distribution into thermal and an excess emission, which is presumably non-thermal. According to Salter *et al.* (1989) and Sievers *et al.* (1991), the flux-densities at $\nu\geq 90$ GHz in Table 6 are purely thermal which can be fitted by an optically-thin thermal free-free emission with $\alpha=-0.1$. We assume that the H II region is isothermal at $T_e=$ 6,400K, which is a mean of previous results (Mezger & Höglund 1967; Mezger & Henderson 1967; Shaver 1969; Terzian & Balick 1969; Hobbs & Johnson 1973; Churchwell *et al.* 1978; Downes *et al.* 1980). If we take the size of the H II region as 2′, determined by previous observations at $\nu>5$ GHz (see Table 6), then the flux-densities at $\nu\geq 90$ GHz yield an emission measure of $EM\simeq 3.5\times 10^6$ pc cm^{-6}. The free-free optical depth $\tau(\nu)$ is given by (Mezger & Henderson 1967),

$$\tau(\nu)=8.235\times 10^{-2}\,(T_e/\mathrm{K})^{-1.35}(\nu/\mathrm{GHz})^{-2.1}(EM/\mathrm{pc\ cm^{-6}}). \quad (8)$$

Hence, the critical density at which the optical depth becomes one is $\nu_c\simeq 1.5$ GHz. The solid line in Figure 10a represents the expected flux-density distribution of *thermal* free-free emission. Note that the thermal flux density at 2.7 GHz obtained in this paper (filled-circle) agrees well with the solid line. Figure 10b shows the residual radio continuum flux-densities (empty-circles), which are presumably non-thermal. At high frequencies of $\nu>15$ GHz, there are negligible residual emissions. The non-thermal continuum flux-density obtained in this paper is marked as filled-circle in Figure 10b, and it agrees with the expected residual emission.

Figure 10b shows that the residual spectrum of G49.5−0.4 cannot be described by a simple power-law. Instead the flux density distribution becomes flat and decreases at $\nu\lesssim 1$ GHz. This low-frequency cut-off is likely due to the absorption by thermal plasma. If the non-thermal source is located within or beyond G49.5−0.4, it is quite possible for the non-thermal emission to be absorbed by thermal plasma because G49.5−0.4 is

Table 6. Continuum Flux-density of G49.5−0.4.

Frequency (GHz)	FWHM	Angular Size	Flux (Jy)	Error (Jy)	Reference[1]
0.15	2′×5′	6.4′×16′	17.2	2.0	1
0.15	2′×5′	5.7′×7.6′	6.8	0.9	1
0.41	2.8′	6.0′×6.9′[2]	43	4.3	2
0.41	(?)	(?)	53.2	7.8	3, 4
0.61	9′	(?)	51	15	5
1.4	10′	3.0′×5.0′	100	(?)	6
2.7	11′	3.0′×5.0′	119	(?)	6
2.7	4.2′	7.0′×6.0′	102	20	7
5.0	11′	3.0′×5.0′	109	(?)	6
5.0	6.5′	4.9′×3.8′[2]	117	(?)	8
5.0	4′	3.0′×3.0′	115	(?)	9
5.0	6.5′	4.7′×3.0′	117	(?)	10
5.0	2.6′	2.2′×2.0′[2]	95	(?)	11, 12
5.0	2.6′	2.6′[2]	105	(?)	13, 12
11	2.8′	1.8′×1.6′	93	9	14
11	4.6′	1.8′×1.5′	89	14	15
15	2′	2.8′×2.5′[2]	72	(?)	16
18	2.7′	1.8′×1.5′	78	14	15
31	3.5′	1.7′×1.4′	65	13	17
32	1.6′	1.8′×1.5′	70	14	15
37	(?)	1.5′×1.4′	72	15	18, 19
90	28″	(?)	62	6	20
142	20″	(?)	59	10	20, 21
230	25″	(?)	56	22	22, 21
230	32″	(?)	56	17	23, 21
236	30″	(?)	56	17	21
300	3.9′	(?)	55	4	24, 21

[1]Reference: (1) Copetti & Schmidt (1991), (2) Shaver (1969), (3) Goss & Shaver (1970), (4) Mufson & Liszt (1979), (5) Terzian & Balick (1969), (6) Altenhoff *et al.* (1970), (7) This Study, (8) Mezger & Henderson (1967), (9) Wilson *et al.* (1970), (10) Reifenstein *et al.* (1970), (11) Churchwell *et al.* (1978), (12) Altenhoff *et al.* (1978), (13) Downes *et al.* (1980), (14) MACLeod & Doherty (1968), (15) Hobbs & Johnston (1971), (16) Schraml & Mezger (1969), (17) Downes, Maxwell & Rinehart (1970), (18) Berlius & Soronchenko (1973), (19) Malkamäki *et al.* (1979), (20) Salter *et al.* (1989), (21) Sievers *et al.* (1991), (22) Schloerb, Snell & Schwartz (1987), (23) Gordon (1987), (24) Chini *et al.* (1984)

[2]The size is FWHM determined by gaussian fitting.

a very dense H II region complex. If the non-thermal source is beyond G49.5−0.4, however, the expected spectrum would have a cut-off at low-frequencies which is much steeper than Figure 10b. In this paper, we consider a simple model in which the non-thermal continuum sources are well mixed with thermal plasma. The flux-density, $S_{\nu,\mathrm{nth}}$, of non-thermal continuum emission emanating from a well-mixed source, if the non-thermal self-absorption is neglected, may be expressed as

$$S_{\nu,\mathrm{nth}} = S_{\nu,0}\left[\frac{1-e^{-\tau(\nu)}}{\tau(\nu)}\right] \tag{9}$$

where $S_{\nu,0} \propto \nu^{\alpha_0}$ is the non-thermal flux-density in the optically-thin limit. Hence, the observed non-thermal spectrum will be $S_{\nu,\mathrm{nth}} \propto \nu^{\alpha_0}$ for $\nu \gg \nu_c$, and $S_{\nu,\mathrm{nth}} \propto \nu^{(\alpha_0+2.1)}$ for $\nu \ll \nu_c$. The parameter ν_c is the critical frequency at which the optical depth becomes a unity. Figure 10c shows the flux-density distribution where the optical-depth effect has been removed, i.e., $S_{\nu,0}$. The flux-density distribution in Figure 10c can be fitted well with a spectral index of $\alpha \simeq -1.0$. Hence, we conclude that G49.5−0.4 produce both thermal and non-thermal emissions. According to our analysis, the thermal and non-thermal luminosities between $\nu = 0.15$ and 300 GHz

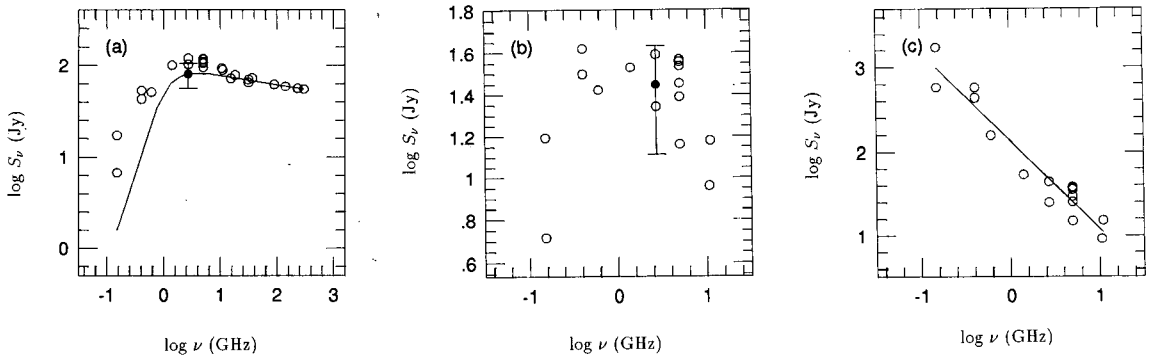

Fig. 10. (a) Flux-density distribution of G49.5−0.4 between $\nu=0.15$ and 300 GHz. The spectral index at $\nu>2$ GHz is $\alpha\simeq-0.18$, whereas at $\nu<2$ GHz, it is $\alpha\simeq0.82$. The solid line represents the expected flux-density distribution of thermal free-free emission derived by a model calculation (see text). Note that the thermal flux-density at 2.7 GHz obtained in this paper (filled-circle with error bar) agrees well with the solid line. (b) Distribution of the residual radio continuum flux-density (empty-circles), which are presumably non-thermal. The non-thermal continuum flux-density obtained in this paper is marked as filled-circle with error bar, and it agrees with the residual emission. The relatively small flux-densities at $\nu<1$ GHz is likely due to the thermal free-free absorption. (c) Same as (b) but the optical-depth effect has been removed. The flux-density distribution is well fitted by a simple power-law $S_\nu\propto\nu^{-1.0}$ (solid line).

are $\sim10^{36}$ and $\sim10^{34}$ ergs s^{-1}, respectively.

What mechanism would be producing the non-thermal emission in G49.5−0.4? First, there could be supernova remnants (SNRs) mixed with the H II region. In some giant H II regions in external galaxies, there are evidences for SNRs mixed with H II regions (Chu & Kennicutt 1986; Gordon *et al.* 1993). For G49.5−0.4, however, this is *not* likely because it is a very young H II region which still undergoes a dynamical collapse of surrounding molecular clouds (Rudolph *et al.* 1990). Secondly, strong stellar winds from O stars could produce such non-thermal emission (White 1985). Bieging, Abbort & Churchwell (1989) have surveyed 88 Galactic OB stars using the VLA and have suggested that strong non-thermal continuum is very common for very luminous stars. The non-thermal emission has a negative spectral index between $\alpha=-0.9$ and -0.3 and luminosities of $\sim10^{19}$ ergs s^{-1}Hz^{-1} at 5 GHz. According to our result, G49.5−0.4 has a luminosity of $\sim10^{23}$ ergs s^{-1}Hz^{-1} at 5 GHz. Therefore, we need $\sim10^4$ number of OB stars to attribute the non-thermal emission from G49.5−0.4 to stellar winds. Even though G49.5−0.4 is one of the most active sites for massive star formation, the required number of OB stars seems to be too large. Hence, the origin of the non-thermal emission from G49.5−0.4 is not certain.

2. G49.1−0.4

G49.1−0.4 is peculiar because it is the only H II region in the W51 complex that does not have an associated molecular clump (Figure 8). Also, high-velocity (HV) H I gas has been detected in this region by Koo & Heiles (1991) using the 26-m telescope at Hat Creek (HPBW$\simeq$36′). The HV H I gas moves at $v_{\rm exp}\simeq95$ km s^{-1} with respect to the rest of gas. The mass and kinetic energy of the HV H I gas are $M_{\rm HI}\simeq5.1\times10^3\,M_\odot$ and $E_{\rm K}\simeq4.8\times10^{50}$ ergs, respectively.

The absence of molecular gas and the existence of HV H I gas may be closely related to each other. We may consider the HV H I gas originated from the dissociation of the molecular gas. If we use the radio continuum flux of G49.1−0.4 and the correlation between the radio continuum flux of H II region and CO flux of associated molecular clump (eq. 6), then the expected mass for molecular clump at G49.1−0.4 may be estimated. However, in Figure 5b, G49.1−0.4 is too weak for its flux to be determined. Instead we extrapolate the 10.6 GHz flux 5.3 Jy of MacLeod & Doherty (1968) using the spectral index of optically-thin thermal emission $\alpha=-0.1$ to derive the 2.7 GHz flux 6.1 Jy of G49.1−0.4. If we substitute $S_{11,\rm th}=6.1$Jy into eq. (6) and the expected mass of a molecular clump is $M_{\rm exp}\sim3\times10^3\,M_\odot$. Considering the uncertainties in mass

estimation, the molecular mass is comparable to the HV H I gas. Hence, presumably, there had been an enough molecular gas to produce the HV H I gas. The association between the HV H I gas and G49.1−0.4 will be studied in a separate paper (Moon & Koo 1994).

3. SNR W51C

In Figure 7b, W51C appears as a large, partially complete shell structure with its northern part opened. The diameter of the shell is ~30′ (or ~44 pc) at a distance of 5 kpc (see next). According to our result, the flux of W51C is $S_\nu \simeq 130 \pm 40$ Jy at 11-cm, which is significantly larger than $S_\nu \simeq 34$ or 51.5 Jy of Altenhoff *et al.* (1970) and Velusamy & Kundu (1974). The difference is due to their small sizes, ≃7′ and 17.3′, in deriving the flux.

In order to derive the spectral index of W51C, we summarize the observed fluxes in Table 7. Columns 1 and 2 contain the frequency and flux of each observation. Columns 3 and 4 contain the size of W51C and reference for each observation. Table 7 lists only the observations with an estimated size greater than ~24′. Figure 11 shows the flux distribution of W51C, where the filled-circle represents the flux obtained in this paper. In the

Table 7. Continuum Fluxes of W51C.

Frequency (GHz)	Flux (Jy)	Size (arcminute)	Reference
0.15	114±17	30	Copetti & Schmidt (1991)
0.40	200±40	24	Downes (1971)
0.41	200±40	27	Shaver (1969)
1.0	160±32	27	Green (1988)
1.4	130±26	24	Downes (1971)
2.7	133±40	30	This Study
5.0	109±22	24	Downes (1971)
5.0	106±22	26	Clark & Caswell (1976)
11	79±16	26	MACLeod & Doherty (1968)

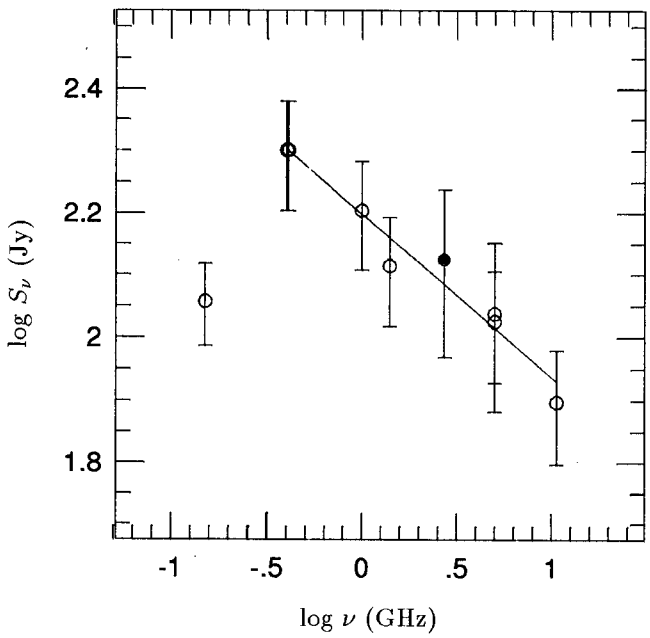

Fig. 11. Flux distribution of W51C between $\nu = 0.15$ and 11 GHz. At $\nu > 0.40$ GHz, the distribution is well described by $S_\nu \propto \nu^{-0.26}$. At 0.15 GHz, the flux deviates significantly, which is possibly due to free-free absorption.

frequency range between $\nu = 0.4$ and 10.7 GHz, it shows a typical non-thermal spectrum of $\alpha \simeq -0.26$ (solid line). At 0.15 GHz, the flux deviates significantly according to Copetti & Schmidt (1991), who argued that the deviation is due to the free-free absorption.

We may use the surface brightness-diameter, $\Sigma - D$, relation to derive an approximate distance to the SNR W51C. If we use the relation given by Berkhuijsen (1986) who used samples in the Galaxy, the Magellanic Clouds, M31, and M33, the distance to W51C is 5.6 kpc. Instead if we divide the foreground H I column density toward G49.0−0.5 in W51C (Table 2), $N_{\rm H\,I} \simeq 8.5 \times 10^{21}$ cm^{-2}, by the mean H I number density 0.57 cm^{-3} (Dickey & Lockman 1990), we obtain a distance of 5 kpc.

VI. SUMMARY

We have decomposed the 11-cm radio continuum emission of the W51 complex into thermal and non-thermal components. The decomposition is based on the correlation between the radio continuum and the 60-μm emissions from H II regions. We have estimated the 60-μm intensity distributions associated with neutral gas $I_{60,\rm n}$ (MJy sr^{-1}) from our Arecibo H I 21-cm line data and the Massachusettes-Stony Brook CO survey data. The 60-μm intensity distribution associated with ionized gas $I_{60,\rm i}$ has been obtained by subtracting $I_{60,\rm n}$ from the IRAS 60-μm data. By comparing the 60-μm map of the ionized component with the 11-cm continuum map, we have found the correlation between $I_{60,\rm i}$ and the 11-cm brightness temperature T_{11} (K). The correlation is used to obtain the 11-cm thermal and non-thermal maps of the W51 complex. In the following, we summarize our main results.

(1) Toward the W51 complex, most (87%) of the 60-μm flux originates from the dusts associated with ionized gas. The remaining 13% is from the dusts associated with atomic (9%) and molecular (4%) gases.

(2) There is a good correlation between $I_{60,\rm i}$ and the 11-cm thermal continuum brightness temperature $T_{11,\rm th}$: $T_{11,\rm th} = (7.9^{+2.1}_{-1.6}) \times 10^{-3}\ I_{60,\rm i}$.

(3) About 65% of the total 11-cm flux toward the W51 complex is thermal, the 65% of which is from the compact H II regions. All the compact H II regions, except G49.1−0.4 in W51B, have associated dense molecular clumps. The mass of stars in compact H II regions M_* is proportional to the mass of associated molecular clump M_c, $M_* \propto M_c^{0.4\pm0.1}$. The star-formation-efficiency of the W51 complex is higher than the average value in the Galactic plane.

(4) The 11-cm non-thermal emission, which constitutes ~35% of the total 11-cm flux, is composed of three sources: a strong compact source at G49.5−0.4 in W51A, a weak compact source close to G49.2−0.3 in W51B, and the extended shell source W51C. The nature of the non-thermal source close to G49.2−0.3 is not known and the reality of the non-thermal emission needs to be confirmed.

(5) G49.5−0.4, which has been known as an H II region complex, has a significant (~25%) non-thermal flux at 11-cm. Its spectral flux-density distribution between 0.15 and 300 GHz also suggests an excess emission over thermal free-free emission. The excess emission can be interpreted as a non-thermal emission from G49.5−0.4, where thermal and non-thermal sources are well-mixed. The non-thermal emission has a steep spectral index $\alpha \simeq -1.0$ ($S_\nu \propto \nu^\alpha$). The luminosity of non-thermal emission (~10^{34} ergs s^{-1}) is negligible compared to that of thermal emission (~10^{36} ergs s^{-1}). The origin of the non-thermal emission is not certain.

(6) G49.1−0.4 is peculiar because it is the only compact H II region in the W51 complex that does not have an associated molecular clump. The physical association between G49.1−0.4 and the previously detected HV H I gas (Koo & Heiles 1991) needs to be studied.

(7) The shell source W51C has a 11-cm flux of ~130 Jy. The spectral index is $\alpha \simeq -0.26$ between 0.4 and 10.7 GHz.

ACKNOWLEDGEMENTS

We are very grateful to John Bieging for his helpful comments. We wish to thank Wolfgang Reich for providing us the Bonn 11-cm survey data. This work has been supported by NON DIRECTED RESEARCH

FUND, Korea Research Foundation, (1992).

REFERENCES

Altenhoff, W. J., Downes, D., Goad, L., Maxwell, A. & Rinehart, R. 1970, A&AS, 1, 319
Altenhoff, W. J., Downes, D., Pauls, T. & Schraml, J. 1978, A&AS, 35, 23
Berkhuijsen, E. M. 1986, A&A, 166, 257
Berulis, I. I. & Sorochenko, R. L. 1973, Sov. Astron., 17, 179
Bieging, J. 1975, in H II Regions and Related Topics, ed. T. L. Wilson & D. Downes (Heidelberg: Springer -Verlag), 443
Bieging, J. H., Abbott, D. C. & Churchwell, E. B. 1989, ApJ, 340, 518
Bloemen, J. B. G. M., Deul, E. R. & Thaddeus, P. 1990, A&A, 233, 437
Broadbent, A., Haslam, C. G. T. & Osborne, J. L. 1989, MNRAS, 237, 381
Chini, R., Kreysa, E., Mezger, P. G. & Gemund, H.-P. 1984, A&A, 137, 117
Chu, Y.-H. & Kennicutt, R. C. 1986, ApJ, 311, 85
Churchwell, E., Smith, L. F., Mathis, J., Mezger, P. G. & Huchtmeier, W. 1978, A&A, 70, 719
Clark, D. H. & Caswell, J. L. 1976, MNRAS, 174, 276
Clemens, D. P. 1985, ApJ, 295, 422
Copetti, M. V. & Schmidt, A. A. 1991, MNRAS, 250, 127
Deshpande, A. A. & Sastry, C. V. 1986, A&A, 160, 129
Dickey, J. M. & Lockman, F. J. 1990, ARA&A, 28, 215
Downes, D. 1971, AJ, 76, 305
Downes, D., Maxwell, A. & Rinehart, R. 1970, ApJ, 161, L123
Downes, D., Wilson, T. L., Bieging, J. & Wink, J. 1980, A&AS, 40, 379
Fürst, E., Reich, W. & Sofue, Y. 1987, A&AS, 71, 63
Garay, G., Reid, M. & Moran, J. M. 1985, ApJ, 289, 681
Gaume, R. A., Johnston, K. J. & Wilson, T. L. 1993, ApJ, 417, 645
Genzel, R., Downes, D., Schneps, M. H., Reid, M. J., Moran, J. M., Kogan, L. R., Kostenko, V. I., Matveyenko, L. I. & Rönnäng, B. 1981, ApJ, 247, 1039
Goldsmith, P. F. 1987 in Interstellar Processes, ed. D. J. Hollenbach & H. A. Thronson (Dordrecht: Reidel), 51
Gordon, M. A. 1987, ApJ, 316, 258
Gordon, K. J., Gordon, C. P. & Lockman, F. J. 1974, ApJ, 192, 337
Gordon, S. M., Kirshner, R. P., Duric, N. & Long, K. S. 1993, ApJ, 418, 743
Goss, W. M. & Shaver, P. A. 1970, Aust. J. Phys. Astrophys. Suppl, 14, 77
Green, E. 1988, Ap&SS, 148, 3
Harper, D. A. & Low, F. J. H. 1971, ApJ, 165, L9
Haslam, C. G. T., Salter, C. J., Stoffel, H. & Wilson, W. E. 1982, A&AS, 20, 37
Haynes, R. F., Caswell, J. L. & Simons, L. W. J. 1978, Aust. J. Phys. Astrophys. Suppl, 45, 1
Ho, P. T. P. & Haschick, A. D. 1981, ApJ, 248, 622
Hobbs, R. W. & Johnston, K. J. 1971, ApJ, 163, 299
Koo, B.-C. & Heiles, C. 1991, ApJ, 382, 204
Koo, B.-C., Heiles, C. & Reach, W. T. 1992, ApJ, 390, 108
Kundu, M. R. & Velusamy, T. 1967, Ann. Ap., 30, 59
MacLeod, J. M. & Doherty, L. H. 1968, ApJ, 154, 833
Malkamäki, L., Sandell, G., Mattila, K. & Gebler, K.-H. 1979, A&A, 71, 198
Martin, A. H. M. 1972, MNRAS, 157, 31
Mezger, P. G. & Henderson, A. P. 1967, ApJ, 147, 471
Mezger, P. G. & Höglund, B. 1967, ApJ, 147, 490
Miller, G. & Scalo, J. 1979, ApJS, 41, 513
Moon, D.-S. & Koo, B.-C. 1994 in preparation

Mufson, S. L. & Liszt, H. S. 1979, ApJ, 232, 451
Myers, P. C., Dame, T. M., Thaddeus, P., Cohen, R. S., Silverberg, R. F., Dwek, E. & Hauser, M. G. 1986, ApJ, 301, 398
Osterbrock, D. E. 1989 in Astrophysics of Gaseous Nebulae and Active Galactic Nuclei, (Mill Valley: University Science Books), 224
Pankonin, V., Payne, H. E. & Terzian, Y. 1979, A&A, 75, 365
Reich, W., Fürst, E., Reich, P. & Reif, K. 1990, A&AS, 85, 633
Reich, W., Reich, P. & Fürst, E. 1990, A&AS, 83, 539
Reifenstein III, F. C., Wilson, T. L., Burke, B. F., Mezger, P. G. & Altenhoff, W. J. 1970, A&A, 4, 35
Rudolph, A., Welch, W. J., Palmer, P. & Dubrulle, B. 1990, ApJ, 363, 528
Salter, C. J., Emerson, D. T., Steppe, H. & Thunn, C. 1989, A&A, 225, 167
Sanders, D. B., Clemens, D. P., Scoville, N. Z. & Solomon, P. M. 1986, ApJS, 60, 1
Schloerb, F. P., Snell, R. L. & Schwartz, P. R. 1987, ApJ, 319, 426
Schneps, M. H., Lane, A. P., Downes, D., Moran, J. M., Genzel, R. & Reid, M. J. 1981, ApJ, 249, 124
Schraml, J. & Mezger, P. G. 1969, ApJ, 156, 269
Scoville, N. Z., Yun, M. S., Clemens, D. P., Sanders, D. B. & Waller, W. H. 1987, ApJS, 63, 821
Seward, F. D. 1990, ApJS, 73, 781
Shaver, P. A. 1969, MNRAS, 142, 273
Sievers, A. W., Mezger, P. G., Gordon, M. A., Kreysa, E., Haslam, C. G. T. & Lemke, R. 1991, A&A, 251, 231
Strong, A. W., Bloemen, J. B. G. M., Dame, T. M., Grenier, I. A., Hermsen, W., Leburn, F., Nyman, L.-A., Pollock, A. M. T. & Thaddeus, P. 1988, A&A, 207, 1
Terzian, Y. & Balick, B. 1969, AJ, 74, 76
Turner, B. E., Balick, B., Cudaback, D. D., Heiles, C. & Boyle, R. J. 1974, ApJ, 194, 279
Velusamy, T. & Kundu, M. R. 1974, A&A, 32, 375
Waller, W. H., Clemens, D. P., Sanders, D. B. & Scoville, N. Z. 1987, ApJ, 314, 397
Wendker, H. & Yang, K. S. 1968, AJ, 73, 61
White, R. L. 1985, ApJ, 289, 698
Wilson, T. L., Mezger, P. G., Gardner, F. F. & Milne, D. K. 1970, Astrophys. Letters, 5, 99
Wilson, T. L., Bieging, J. & Wilson, W. E. 1979, A&A, 71, 205
Wood, D. & Churchwell, E. 1989, ApJS, 69, 31